

Oscillation-Based energy Harvester Using Aerodynamic ambient Airflow For Wireless Sensor

**Umoren Mfonobong
Anthony¹**

*Department of
Electrical/Electronic and
Computer Engineering
University of Uyo
mfon4gigisisi@yahoo.com*

**Okafor Ephraim
Chimela²**

*Federal University of Technology
(FUTO) Owerri, Imo State
Nigeria*

Kufre M. Udofia³

*Department of Electrical/Electronic
and Computer Engineering
University of Uyo*

Abstract— In this paper, modelling of a piezoelectric energy harvester to harness aerodynamic energy from airflow is presented. Notably, distributed-parameter models of a piezoelectric energy harvester using an oscillating or dynamic airfoil wing as a base structure and attached to a bimorph piezoelectric cantilevered beam is developed. The source of ambient vibration is a wind induced dynamic flutter which was found to initiate at a low airflow speed of 3.25 m/s. Modelling of the bimorph cantilevered piezoelectric harvester was performed based on the Euler-Bernoulli beam theory and the airfoil stability analysis was carried out using p – k method. A maximum power output of 5728mW and 23.227mW was obtain from plunge and pitch configuration respectively, at a resonance frequency of 854.80 Hz. Hence, the airfoil plunge piezo-aeroelastic energy harvester gave a substantial improvement in power generation at low wind speed capable of supporting many wireless sensor applications without need for incorporating energy storage device within the system.

Keyword: Piezo-aeroelastic Energy Harvester; Airfoil; Cantilever beam; Energy Harvester; Vibration; Pitch; Plunge.

I. INTRODUCTION

Energy harvesting (EH) is the process where electrical energy is obtained from external ecological or natural sources (such as solar power, heat energy, atmospheric wind energy, motion, salinity gradients, water waves, kinetic energy and vibrations), and other sources of energy like the human body as well as chemical and biological sources [1, 2, 3, 4]. In EH, energy is captured and stored for low-powered electronic devices like those utilized in portable integrated circuit technological devices and wireless sensors [5]. The harvester produces very little level of electrical power for microelectronic devices and small energy electronics [6, 7].

The benefits of energy harvesting have generated interest in battery-free electronic devices. This means that devices can harvest energy from the environment and directly power the load in a sustainable and efficient manner [8]. The battery-free operation enables new classes of applications in medical devices, environmental and hard to reach places, pipeline monitoring, smart buildings and medical implants [9].

There are many energy harvesting sources available such as thermal, vibration, radio frequency (RF) and solar energy. Different types of energy harvesting sources are shown in Figure 1. Vibration is considered a good energy source especially in industrial application where high voltage can be generated with moderate power density [10, 11, 12]

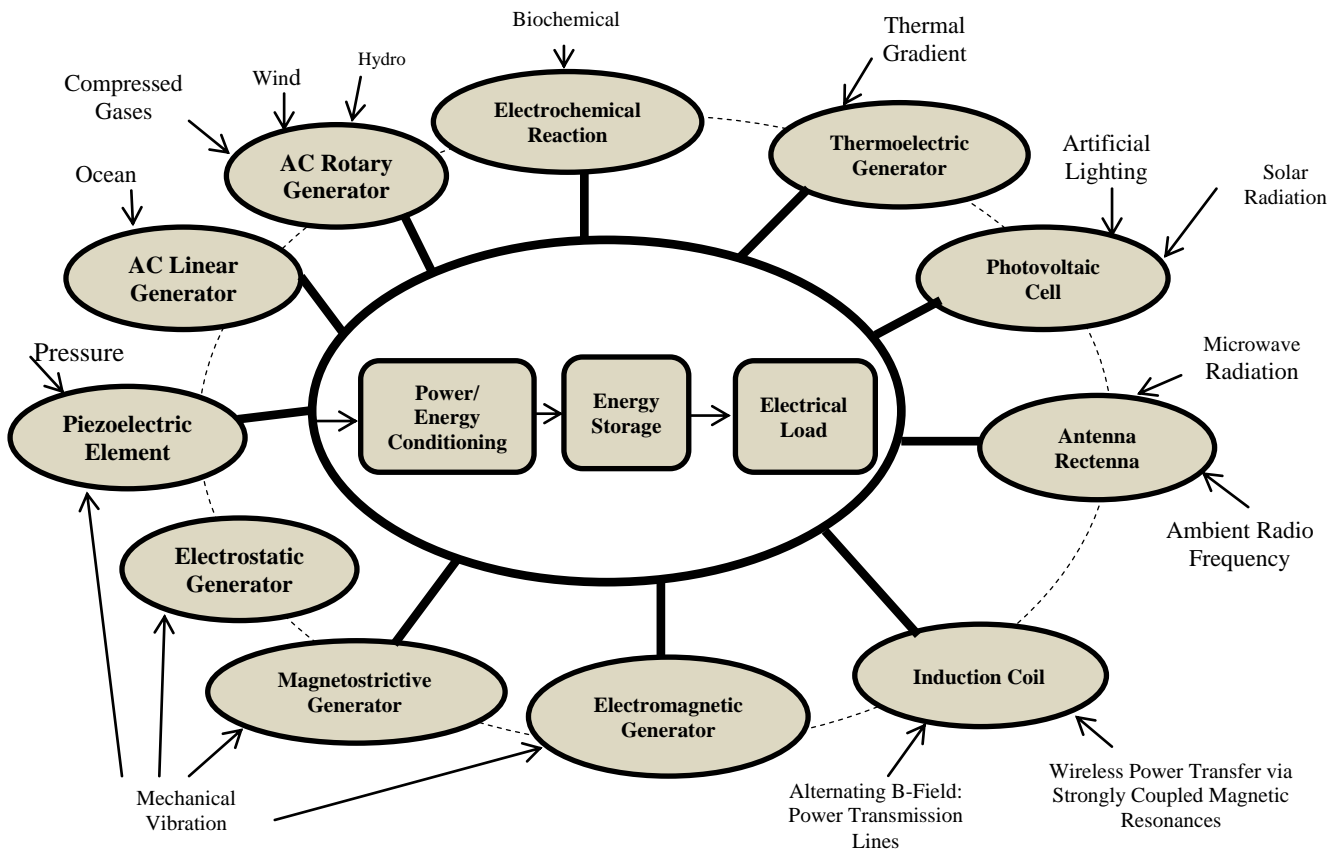


Figure 1. : Energy harvesting sources and their energy harvester [13]

II. Methodology

A. PIEZOELECTRIC ENERGY HARVESTER MODELLING

The proposed model is a bimorph cantilevered piezoelectric beam mounted on a trailing edge of an airfoil shaped wing attached to a base structure, as shown in

Figure 2. In the figure, the piezoelectric cantilever beam has a tip mass placed at the end of the beam. The vibration in the beam is transferred from an airfoil wing which is undergoing moderate flutter phenomenon due to air flow streams over the wing. The simplified aeroelastic system consist of a rigid two-dimensional airfoil mounted on torsional (pitch motion) and translational (plunge motion) springs.

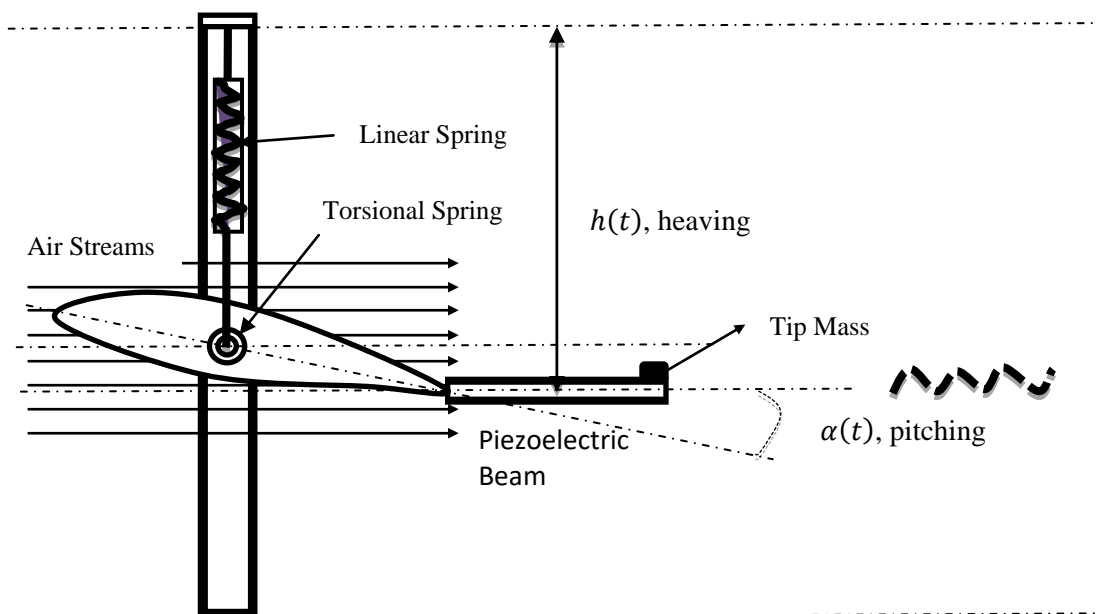


Figure 2: Cross sectional view of piezoelectric energy harvester setup

It is convenient to derive its forced response when the system is subjected to a series of harmonic excitations from aerodynamic force. The undamped response frequency response function (FRFs) of the 2-DoF (degree of freedom) in both plunge ($h(t)$) and pitch ($\alpha(t)$) can be obtained from equation (1) and (2) as [14]:

$$h(t) = \frac{1}{|H_{11}H_{22} - H_{12}H_{21}|} |H_{11} - H_{21}| F_0 e^{j\omega t} \quad (1)$$

$$\alpha(t) = \frac{1}{|H_{11}H_{22} - H_{12}H_{21}|} |H_{22} - H_{12}| F_0 e^{j\omega t} \quad (2)$$

where the element of the undamped response FRFS in both plunge and pitch are:

$$\begin{aligned} H_{11} &= (1 - \pi\rho c)\omega^2 + \left(\frac{\bar{\omega}}{U}\right)^2 K_h - 2\pi\rho V c C(k), H_{12} = \\ & (x_a + \pi\rho c^2 \alpha_h)\omega^2 + \left(\frac{\bar{\omega}}{U}\right)^2 K_h - [\pi\rho c V + 2\pi\rho V c (0.5 - \\ & \alpha_h)]j\omega - 2\pi\rho V^2, H_{21} = \left(\frac{x_a}{r_\alpha} + \pi\rho c^2 \alpha_h\right)\omega^2 - \\ & 2\pi\rho V c (0.5 - \alpha_h) C(k), H_{22} = \left(1 - \pi\rho c^3 \left[\left(\frac{1}{8} + \right. \right. \right. \\ & \left. \left. \left. \alpha_h^2\right)\right]\right)\omega^2 - \pi\rho c^2 V (0.5 - \alpha_h)j\omega + \left(\frac{1}{U}\right)^2 K_\alpha \end{aligned} \quad (3)$$

The undamped airfoil plunge motion has complex aerodynamic amplitude under quasi-steady condition and given as:

$$\begin{aligned} H_1 &= \\ & c \left[\left((1 - \pi\rho c - x_a - \pi\rho c^2)\omega^2 + \left(\frac{\bar{\omega}}{U}\right)^2 K_h - g(1+V) \right) \right] + c[\pi\rho V + 2\pi\rho c e]j\omega \\ & \left[(1 - \pi\rho c) \left(1 + \frac{K_h}{U^2} \right) \omega^2 + \left(\frac{\bar{\omega}}{U}\right)^2 K_h - g \right] (1 - \pi\rho c^3 f) \omega^2 + K_\alpha \left(\frac{\bar{\omega}^2}{U^4} K_h - g \right) - \\ & \left[\left(\left(\frac{x_a}{r_\alpha} + \pi\rho c^2 \alpha_h \right) \omega^2 - g e \right) \left((x_a + \pi\rho c^2 \alpha_h) \omega^2 - 2\pi\rho V^2 \right) \right] + \\ & \left[\left(\pi\rho c^2 (1 - \pi\rho c) \omega - \left(\frac{\bar{\omega}}{U}\right)^2 K_h \pi\rho c^2 + g^2 e \right) - \left(\frac{x_a}{r_\alpha} + \pi\rho c^2 \alpha_h \right) \omega^2 + g \right] \pi\rho c (V + 2e) j\omega \end{aligned} \quad (4)$$

The undamped airfoil pitch motion has complex aerodynamic amplitude under quasi-steady and given as:

$$\begin{aligned} \alpha_1 &= \\ & \frac{c \left[\left((1 - \pi\rho c^3) - (x_a + \pi\rho c^2 \alpha_h) \right) \omega^2 + \left(2\pi\rho V^2 + \frac{K_g}{U^2} \right) \right] + \pi\rho c^2 [(V + 2e) - cV e] j\omega}{\left[(1 - \pi\rho c) \left(1 + \frac{K_h}{U^2} \right) \omega^2 + \left(\frac{\bar{\omega}}{U}\right)^2 K_h - g \right] (1 - \pi\rho c^3 f) \omega^2 + K_\alpha \left(\frac{\bar{\omega}^2}{U^4} K_h - g \right) -} \\ & \left[\left(\left(\frac{x_a}{r_\alpha} + \pi\rho c^2 \alpha_h \right) \omega^2 - g e \right) \left((x_a + \pi\rho c^2 \alpha_h) \omega^2 - 2\pi\rho V^2 \right) \right] + \\ & \left[\left(\pi\rho c^2 (1 - \pi\rho c) \omega - \left(\frac{\bar{\omega}}{U}\right)^2 K_h \pi\rho c^2 + g^2 e \right) - \left(\frac{x_a}{r_\alpha} + \pi\rho c^2 \alpha_h \right) \omega^2 + g \right] \pi\rho c (V + 2e) j\omega \end{aligned} \quad (5)$$

where: ρ is air density, c is the length of the airfoil semi-chord, C or $C(k)$ theodorsen function, ω is the frequency of oscillations, μ is the airfoil-air mass ratio, $\bar{\omega}$ is the frequency ratio, K_h is the linear restoring force, x_a is the nondimensional distance from elastic axis to center of mass, V is the velocity of air speed, k_a is the air damping coefficient, α_h is the nondimensional distance measured from airfoil mid-chord to elastic axis, F_0 is the initial harmonic force amplitude of the forced aeroelastic system, U is the nondimensional airspeed, r_α is nondimensional radius of gyration about elastic axis, $e = (0.5 - \alpha_h)$, $f = \left(\frac{1}{8} + \alpha_h^2\right)$, and $g = 2\pi\rho V c C(k)$.

B. COUPLED ELECTRICAL CIRCUIT FOR PARALLEL CONNECTION OF PIEZOCERAMIC LAYERS

This section presents the closed-form expressions for the coupled electrical and mechanical response of the energy harvester of the bimorph parallel configuration of piezoceramic layers shown in Figure 2. These will include the closed-form voltage, $v_p(t)$, current, $i_p^p(t)$ and electrical power, $P_p(t)$ responses of the piezoelectric energy harvester under modal excitation of the airfoil base structure. The coupled circuit equation can then be obtained from the circuit diagram shown in Figure 3.

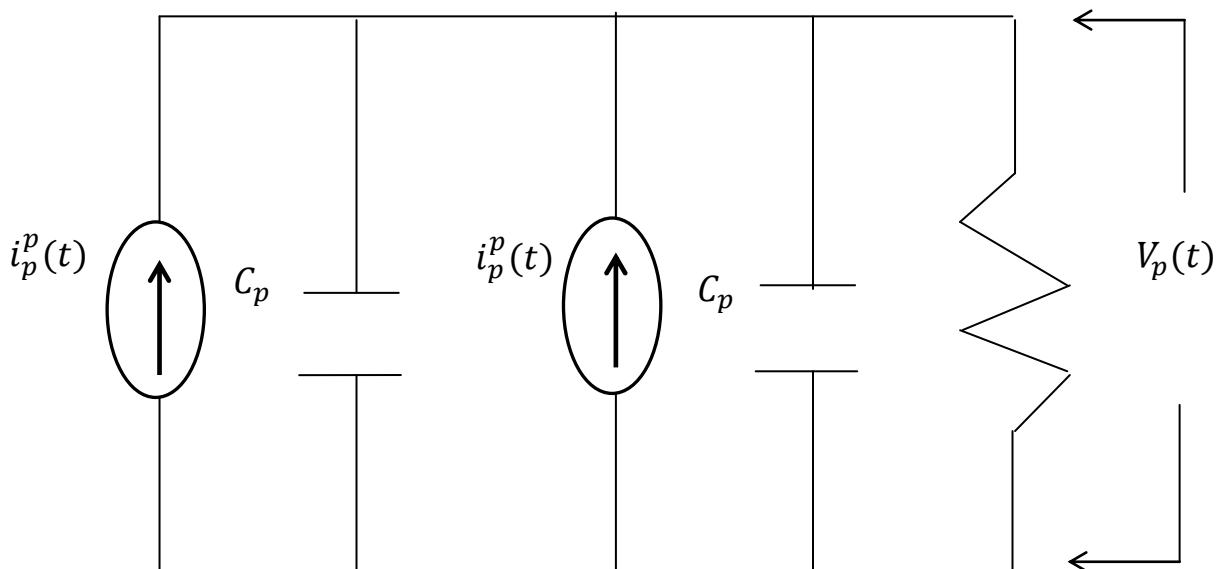


Figure 3.: Electrical circuit for parallel connection of the piezoceramic layer elements

Each piezoceramic layer can be represented as a current source in parallel with its internal capacitance, and the effective capacitance of the electrical circuit becomes [15]:

$$C_p + C_p = 2C_p \quad (6)$$

This can then be used to derive the governing electrical circuit equation based on the Kirchhoff laws; the coupled electrical circuit equation of parallel piezoelectric layers is given as [15]:

$$2C_p \frac{dv_p(t)}{dt} + \frac{v_p(t)}{R_l} = i_p^p(t) \quad (7)$$

Comparing Equations (6) and (7), the internal capacitance and the current source terms of the bimorph for each layer are given as [15]:

$$C_p = \frac{\bar{\epsilon}_{33} b L}{2 h_p}, i_p^p(t) = \varphi_{nr} \sum_{r=1}^{\infty} \frac{d\eta_{br}^p(t)}{dt} \quad (8)$$

where: $\varphi_{nr} = -\bar{\epsilon}_{31} h_{pc} b \int_0^L \frac{\partial^3 w_r(x,t)}{\partial x^2 \partial t} = -\frac{\bar{\epsilon}_{31} (h_p + h_s) b}{2} \left[\frac{d\phi_{br}(x)}{dx} \right]_{x=L}$, ϕ_{br} is the mass-normalized eigenfunction of the r th vibration mode, $\bar{\epsilon}_{33}^S$ is the permittivity component at constant strain, L is the length of the piezoelectric layer, b is the width, h_p is the thickness of each piezoelectric layer, h_s is the thickness of the substructure layer, C_p is the internal capacitance and $\eta_{br}^p(t)$ is the mechanical response.

C. PIEZOELECTRIC ENERGY HARVESTER RESPONSES UNDER STEADY STATE AIRFOIL AERODYNAMIC EXCITATIONS

The major contribution of the acceleration comes from the modal aerodynamic forcing function. The plunge and the pitch displacements of the airfoil are given by $h(t) = H_1 F_0 e^{\frac{j\omega V}{c} t}$ and $\alpha(t) = \alpha_1 F_0 e^{\frac{j\omega V}{c} t}$ where H_1 and α_1 are the steady state complex value for plunge and pitch displacement aerodynamic constants, F_0 is the coupled aerodynamic force amplitude, V is free stream air speed, c is the length of the airfoil semi-chord and ω is the excitation frequency.

The modal force amplitude can be expressed as :

$$F_{ts} = \frac{\omega^2 V^2 F_0}{c^2} \left[m \left(H_1 \int_0^L \phi_{br}(x) dx + \alpha_1 \int_0^L x \phi_{br}(x) dx \right) + m_t \phi_{br}(L) (H_1 + L \alpha_1) \right] \quad (9)$$

The complex modal forcing amplitudes for pitch and plunge steady state aerodynamics are given as follows:

$$F_{ts} = \frac{\omega^2 V^2 F_0}{c^2} Q_{rs} H_1 + \frac{\omega^2 V^2 F_0}{c^2} \Phi_{rs} \alpha_1 \quad (10)$$

where:

$$Q_{rs} = m \int_0^L \phi_{br}(x) dx + m_t \phi_{br}(L) \quad (11)$$

$$\Phi_{rs} = m \int_0^L x \phi_{br}(x) dx + m_t \phi_{br}(L) \quad (12)$$

D. FREQUENCY RESPONSE OF THE VOLTAGE OUTPUT

The steady-state voltage response can be written in terms of airfoil plunge motion acceleration, pitch motion acceleration, for quasi-steady aerodynamics as:

$$v_{ps,h}(t) = \frac{\sum_{r=1}^{\infty} \frac{j\omega \varphi_{nr} Q_{rs}}{(\omega_{nr}^2 - \omega^2 + j\zeta_r \omega_{nr} \omega)}}{\frac{1}{2R_l} + j2\omega C_p + \sum_{r=1}^{\infty} \frac{j\omega \varphi_{nr} (\chi_p)^2}{(\omega_{nr}^2 - \omega^2 + j\zeta_r \omega_{nr} \omega)}} \left(\frac{V^2 F_0}{c^2} H_1 \right) \quad (13)$$

$$v_{ps,\alpha}(t) = \frac{\sum_{r=1}^{\infty} \frac{j\omega \varphi_{nr} \Phi_{rs}}{(\omega_{nr}^2 - \omega^2 + j\zeta_r \omega_{nr} \omega)}}{\frac{1}{2R_l} + j2\omega C_p + \sum_{r=1}^{\infty} \frac{j\omega \varphi_{nr} (\chi_p)^2}{(\omega_{nr}^2 - \omega^2 + j\zeta_r \omega_{nr} \omega)}} \left(\frac{V^2 F_0}{c^2} \alpha_1 \right) \quad (14)$$

where: χ_p is the modal electromechanical coupling term for parallel connection. χ_p can be written as: $\chi_p = -2\bar{\epsilon}_{31} b h_{pc} \left. \frac{d\phi_{br}(x)}{dx} \right|_{x=L}$.

E. FREQUENCY RESPONSE OF THE CURRENT OUTPUT

In order to derive the expression for the current response, it is pertinent to recall from Ohm's law. Hence, the steady state current FRF under airfoil undamped plunge and pitch acceleration is given as:

$$i_{rps,h}^s(t) = \frac{1}{R_l} \left(\frac{\sum_{r=1}^{\infty} \frac{j\omega \varphi_{nr} Q_{rs}}{(\omega_{nr}^2 - \omega^2 + j\zeta_r \omega_{nr} \omega)}}{\frac{1}{2R_l} + j2\omega C_p + \sum_{r=1}^{\infty} \frac{j\omega \varphi_{nr} (\chi_p)^2}{(\omega_{nr}^2 - \omega^2 + j\zeta_r \omega_{nr} \omega)}} \right) \left(\frac{V^2 F_0}{c^2} H_1 \right) \quad (15)$$

$$i_{rps,\alpha}^s(t) = \frac{1}{R_l} \left(\frac{\sum_{r=1}^{\infty} \frac{j\omega \varphi_{nr} \Phi_{rs}}{(\omega_{nr}^2 - \omega^2 + j\zeta_r \omega_{nr} \omega)}}{\frac{1}{2R_l} + j2\omega C_p + \sum_{r=1}^{\infty} \frac{j\omega \varphi_{nr} (\chi_p)^2}{(\omega_{nr}^2 - \omega^2 + j\zeta_r \omega_{nr} \omega)}} \right) \left(\frac{V^2 F_0}{c^2} \alpha_1 \right) \quad (16)$$

F. FREQUENCY RESPONSE OF THE POWER OUTPUT

The expression for the power response or generated power can be gotten with the relationship between the voltage response, current response and the electrical resistive load in the circuit. The FRFs for airfoil plunge motion acceleration, under quasi-steady aerodynamics is given as:

$$P_{rps,h}^p(t) = \frac{1}{R_l} \left(\frac{\sum_{r=1}^{\infty} \frac{j\omega \varphi_{nr} Q_{rs}}{(\omega_{nr}^2 - \omega^2 + j\zeta_r \omega_{nr} \omega)}}{\frac{1}{2R_l} + j2\omega C_p + \sum_{r=1}^{\infty} \frac{j\omega \varphi_{nr} (\chi_p)^2}{(\omega_{nr}^2 - \omega^2 + j\zeta_r \omega_{nr} \omega)}} \right)^2 \left(\frac{V^2 F_0}{c^2} H_1 \right) \quad (17)$$

$$P_{rps,\alpha}^p(t) = \frac{1}{R_l} \left(\frac{\sum_{r=1}^{\infty} \frac{j\omega \varphi_{nr} \Phi_{rs}}{(\omega_{nr}^2 - \omega^2 + j\zeta_r \omega_{nr} \omega)}}{\frac{1}{2R_l} + j2\omega C_p + \sum_{r=1}^{\infty} \frac{j\omega \varphi_{nr} (\chi_p)^2}{(\omega_{nr}^2 - \omega^2 + j\zeta_r \omega_{nr} \omega)}} \right)^2 \left(\frac{V^2 F_0}{c^2} \alpha_1 \right) \quad (18)$$

The bimorph cantilever beam used in this research is made with apiezoceramic layer of PZT (lead zirconate titanate)

ceramic material with PIC-151 specification as shown in Table 1.

Table 1: Geometric material and electromechanical parameter of PZT.

	Piezoceramic (PIC-151)	Substructure (Copper)
Length (L) [mm]	30	30
Width (b) [mm]	5	5
Thickness (h_p, h_s) [mm]	0.150	0.05
Elastic modulus (c_{11}^E, Y_s) [GPa]	10.0	68.9
Mass density (ρ_p, ρ_s) [kg/m ³]	7800	2700
Piezoelectric constant (e_{31}) [C/m ²]	-2.1	-
Permittivity constant (ϵ_{33}^S) [nF/m]	18.3	-
Mass (m) [kg/m]	0.01394	
Tip Mass (m_t) [kg]	0.50	
Tip Mass Inertia (I_t) [kg]	6.2083×10^{-6}	

The airfoil Eppler E837, wing shaped was selected from the database of University of Illinois, United States of America. This airfoil, tested under Mach number of zero with a maximum thickness of 9.1% at 31.1% of the chord length, and maximum camber of 3.2% at 44.8% chord length as shown in Table 2.

Table 2: Geometric properties of Eppler E387 airfoil

Geometric and Material Properties	Airfoil E387 Wing
Chord, c	75 mm
Span, s	150 mm
Maximum Thickness, t_m	0.091cat 31.1% of c
Maximum Camber, t_c	0.032cat 44.8% of c
Material	Aluminium
Density, ρ_a [kg/m ³]	2700

G. UNCOUPLED AIRFOIL WING ANALYSIS UNDER QUASI-STEADY CONDITIONS

Using MATLAB, codes were generated to predict the flutter speed and flutter using p-k method, throughout the freestream or airflow speed range of consideration, where $V = [0 - 25]m/s$. The properties of the aerodynamic flow condition are given as non-dimensional and dimensional parameters which are: $x_a = 0.5$, $a_h = -0.25$, $\omega_h = 1.3450$, $\omega_a = 16.5655$ and $\bar{\omega} = \frac{\omega_h}{\omega_a} = 0.0812$. The plunge motion of the airfoil response which is equivalent to the torsional spring constant is varied from $K_\alpha = 0.1$ to $0.5 Nm$ and the pitch motion of the airfoil response which is equivalent to the linear spring constant is

varied from $K_h = 1.5$ to $21.5 N/m$. The optimum values that gives the lowest possible frequency ($F_f = 18.36 Hz$) and flutter speed ($V_f = 3.2475 m/s$) for both the linear and torsional spring coefficients are $K_h = 1.5$ and $K_\alpha = 0.1$ respectively.

H. Mode Shape

The analysis given here considers the frequency range from 0 to 1000 Hz. The first three mechanical and electrical resonance frequencies of the bimorph cantilever were obtain from matlab simulation as: $f_{r1} = 94.76 Hz$, $f_{r2} = 379.07 Hz$ and $f_{r3} = 852.90 Hz$ (where $f_r = \omega_{nr}/2\pi$). The optimum aerodynamic parameters were determined for the quasi-steady excitation of the airfoil base. With consideration on the first three vibration modes, the fundamental mode of vibration as shown in Figure 4.

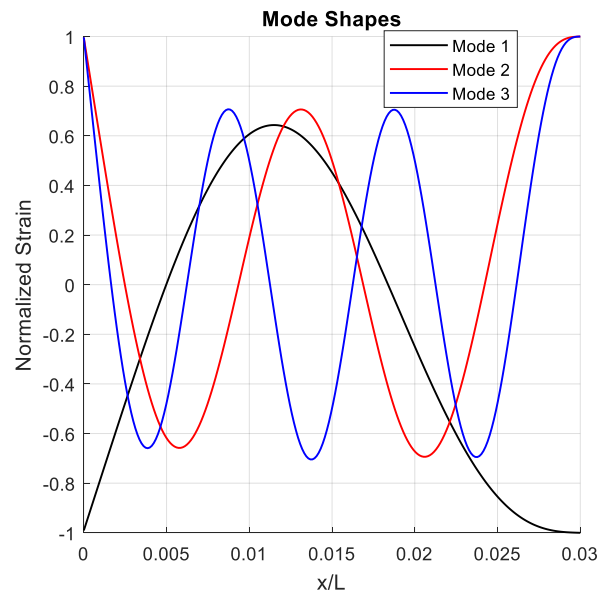


Figure 4 First three vibration mode shapes of energy harvester cantilevered beam

III. RESULTS AND DISCUSSION

In the simulations, the base of the cantilever is assumed to be oscillating as the airfoil either pitch and plunged. The set of electrical load resistance considered here ranges from $1 \mu\Omega$ to $10 M\Omega$. As far as the fundamental vibration mode of this particular bimorph is concerned, the lowest resistance ($R_l = 1 \mu\Omega$) used is very close to the short-circuit condition whereas the largest load ($R_l = 10 M\Omega$) is very close to the open-circuit conditions.

A. FREQUENCY RESPONSE OF VOLTAGE OUTPUT UNDER QUASI-STEADY AERODYNAMIC AIRFOIL BASE EXCITATION

The behaviour of the voltage as the load resistance is increased from short-circuit to open-circuit conditions, remains monotonic at each frequency as shown in Figure 5.

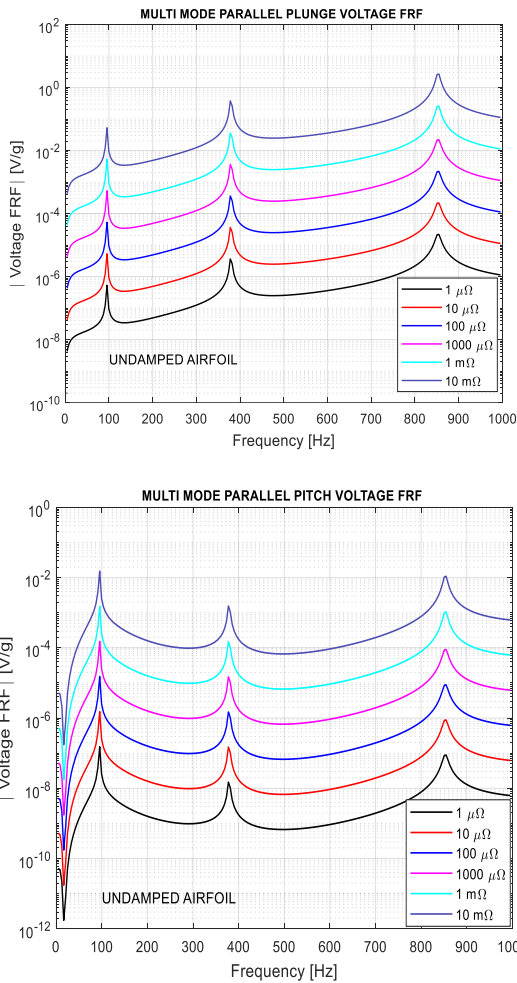


Figure 5: Steady state plunge (a) and pitch (b) voltage FRFs of the bimorph for a specific range of load resistance with undamped airfoil

The voltage FRFs of plunge motion contribution to the voltage FRFs output is basically higher than the pitch motion quota from aerodynamic excitation of the airfoil base structure under quasi-steady conditions. The maximum generated voltage output at each resonance frequency of the system is presented in Table 3. For the plunge motion, the third mode produces the highest voltage contribution $V = 257.30 \text{ mV}$ for the pitch motion, mode one registered a high voltage FRF output of $V = 1.53 \text{ mV}$.

Table 3: Maximum voltage FRFs output of the undamped bimorph piezoelectric aeroelastic energy harvester at resonance frequencies of the first three modes

Mode (r)	f_r [Hz]	Plunge Voltage [mV]	Pitch Voltage [mV]
1	95.44	5.29	1.53
2	377.60	37.73	0.16
3	854.80	257.30	1.09

B. FREQUENCY RESPONSE OF THE CURRENT OUTPUT UNDER QUASI-STEADY AERODYNAMIC AIRFOIL BASE EXCITATION

Unlike the voltage FRF the amplitude of the current at every frequency decreases with increasing load resistance as shown in Figure 6. As the airfoil is excited at every excitation frequency, the maximum value of the current is obtained when the system is close to short-circuit conditions, and minimum when it is at open-circuit, indicating the current is inversely proportional to the load resistance.

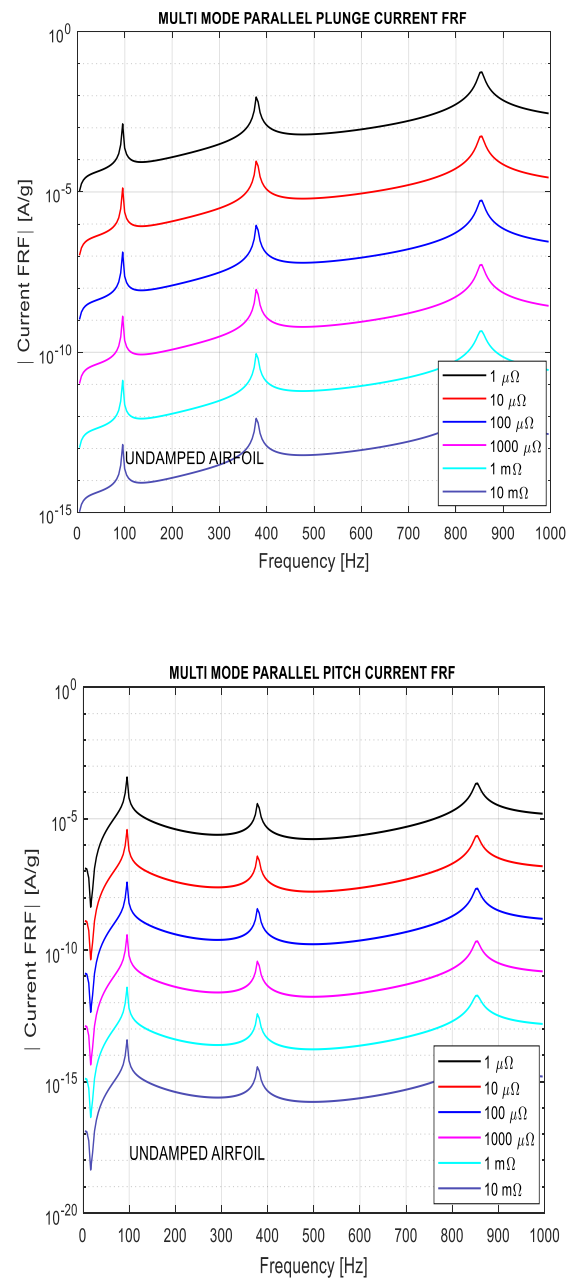


Figure 6: Steady state plunge (a) and pitch (b) current FRFs of the undamped bimorph for a specific range of load resistance

Table 4: Maximum current FRFs output of the bimorph piezoelectric aeroelastic energy harvester at resonance frequencies of the first three modes

Mode (r)	f_r [Hz]	Plunge Current [mA]	Pitch Current [mA]
1	95.44	0.132	0.0381
2	377.60	0.906	0.00374
3	854.80	5.453	0.0222

Figure 6 indicates that the plunge motion contributes more current than the pitch motion of the airfoil base structure. For the plunge motion, the third mode produces the highest current contribution $I = 5.453 \text{ mA}$ while for the pitch motion, mode one registered a high current FRF output of $I = 0.0381 \text{ mA}$.

C. FREQUENCY RESPONSE OF THE POWER OUTPUT UNDER QUASI-STEADY AERODYNAMIC AIRFOIL BASE EXCITATION

The power output is proportional to the square of the voltage output and inversely proportional to the load resistance. The amplitude of the power output at every frequency increases with increasing load resistance but also interwoven at around the first resonance frequency as shown in Figure 7. The maximum value of the power is obtained when the system is close to open-circuit conditions and minimum when it is at short-circuit, and this behaviour analogous to voltage FRFs.

As in the case of voltage and current FRFs with parallel connections, it is also observed that in the power FRFs that the plunge motion contribution to the power FRFs output is higher than the pitch motion portion from aerodynamic excitation of the airfoil base structure under quasi-steady conditions. For the three mode of vibration, the maximum generated power output at each resonance frequency of the system is tabulated in Table 5. For the plunge motion, the third mode produces the highest power $P = 5728.00 \text{ mW}$.

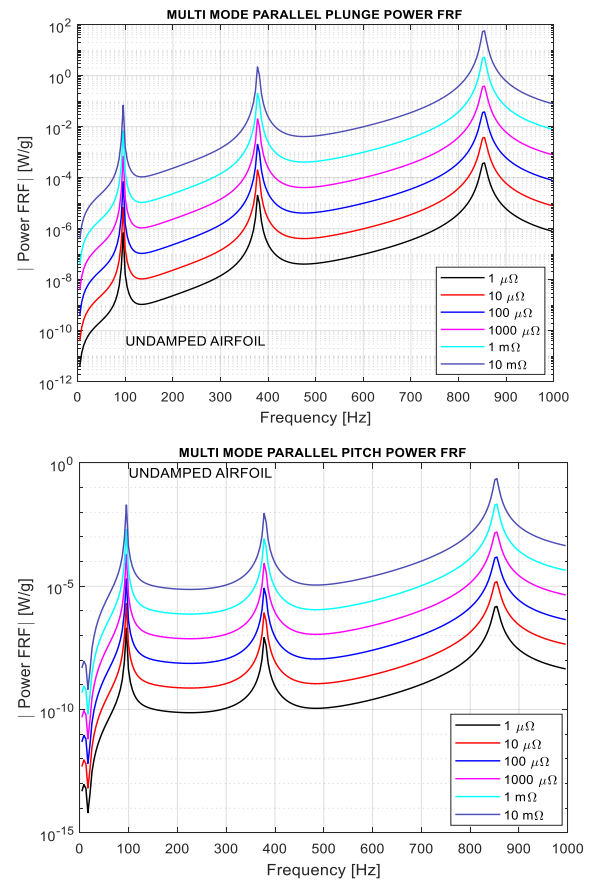


Figure 7: Steady state plunge (a) and pitch (b) power FRFs of the undamped bimorph for a specific range of load resistance

Table 5: Maximum power FRFs output of the undamped bimorph piezoelectric aeroelastic energy harvester at resonance frequencies of the first three modes

Mode (r)	f_r [Hz]	Plunge Power [mW/g]	Pitch Power [mW/g]
1	95.44	6.88	1.99
2	377.60	218.90	0.90
3	854.80	5728.00	23.27

IV. CONCLUSION

This work has addressed the analytical modelling of piezoelectric bimorph cantilever energy harvester using ambient airflow based on Euler-Bernoulli beam theory. The harvester is assumed to be excited due to the oscillating force applied at the beam in the transverse direction. The research has demonstrated that the piezo-aeroelastic energy harvester developed is well suited for deployment in very low wind speed areas. Besides, it has been illustrated that the interaction of the dynamics of airfoil base structure with the bimorph composite beam structural dynamics caused

introduction of strain nodes in the first vibration mode and cancellation of the same in higher modes, resulting in generation of maximum power in mode three and lower energy in mode one. The maximum power outputs of the plunge connection and pitch configuration cases are not identical due to the different aerodynamic condition of excitation of the base structure. It would be an amazing breakthrough, once the models and design are validated experimentally.

REFERENCES

1. Akorode, M. F., Ibrahim, O., Amuda, S. A., Otuze, A. O. and Olufeagba, B. J. (2017). Current Status and Outlook of Renewable Energy Development in Nigeria. *Nigeria Journal of Technology (NIJOTECH)*, 36(1):196-212.
2. Sherazi, H. H., and Grieco, L. A. and Boggia, G. (2018). A comprehensive Review on Energy Harvesting MAC Protocols in WSNs: Challenges and Tradeoffs, *Ad Hoc Network*. (71): 117-134.
3. Rashid, A., Khan, F., Gul, T., Fakhr-e-Alam, Ali S., Khan, S. and Khalil, F. K. (2018). Improving Energy Conservation in Wireless Sensor Networks using Energy harvesting System. *International Journal of Advanced Computer Science and Applications*. 9(1): 1-8.
4. Leon-Gil, J.A., Cortes-Loredo, A., Fabian-Mijangos, A., Martinez-Flores, J. J., Tovar-Padilla, M., Cardona-Castro, M. A., Morales-Sanchez, A., and Alvarez-Quintana, J. (2018) Medium and Short Wave RF Energy Harvester for Power Wireless Sensor network. *Sensors*, 19: 1-13
5. Rizman, Z. I., Yassin I.M., Zaman, F. K., Hashim, F. R., and Yeap, K. H. (2018). Smart Multi-Application Energy Harvesting Using Arduino, *Journal of Fundamental and Applied Science*, (10): 689-704
6. Hu, Y., Xue, H. and Hu, H. (2014). A Piezoelectric Power Harvester with Adjustable Frequency through Axial Preloads. *Smart Materials and Structures*, 16(5): 1961–1966.
7. Podder, P., Constantinou, P., Amann, A. and Roy, S, (2016). Frequency Adjustable MEMS vibration Energy Harvester, *Journal Physics: Conference Series*. (757): 1-6.
8. Mitcheson, P.D., Green, T.C., Yeatman, E.M. and Holmes, A.S. (2014). Architectures for Vibration-driven Micro-power Generators. *Journal of Microelectromechanical Systems*, 13(3): 429- 440.
9. Bradai, S., Naifar, S., Viehweger, C. and Kanoun, O. (2018). Electromagnetic Vibration Energy Harvesting for Railway Applications. *NATEC Web Conferences*, 148(12004): 1-4.
10. Sarker, M., Mohamed, A. and Mohamed, R. (2016). A New Method for a Piezoelectric Energy Harvesting System Using a Backtracking Search Algorithm-based PV Voltage Controller. *Micromachines*, 7(171): 1-16
11. Chiu, X., Kuo, M. and Chu, L. (2017). A Self-Powered Mechanical Strain Energy Sensor. *Smart Materials and Structures*, 10(2): 293-299.
12. Stein, A. L.F and Hofmann, H. F. (2017). Autonomous Wideband Piezoelectric Energy Harvesting Utilizing a Resonant Inverter. *IEEE Transactions on Power Electronics*, 32(8): 6178-6187.
13. Tan, V. K. (2013). Energy Harvesting Autonomous Sensor Systems. Design, Analysis and Practical Implementation. *New-york: Taylor and Francis Group*.
14. Alighanbari, H. (1995). *Flutter Analysis and Chaotic Response of an Airfoil Accounting for Structural Nonlinearities*. PhD Thesis, McGill University, Canada, 24-25p
15. Erturk, A. and Innam, D. J. (2011). *Piezoelectric Energy Harvesting*. John Wiley & Sons, Delhi, 67-71pp.